# Microstructural and Bulk Characterization of Two Poly(siloxane-imide) Multiblock Copolymers

RICHARD J. SPONTAK and MICHAEL C. WILLIAMS,* *Center for Advanced Materials, Lawrence Berkeley Laboratory, Berkeley, California 94720-9989 and Department of Chemical Engineering, University of California, Berkeley, California 94720-9989*

## Synopsis

Much of the unique thermomechanical behavior of microphase-separated block copolymers is well established for the diblock and triblock architectures, and most of the data base involves polymers with polystyrene and polydiene blocks. However, there have been few reports about phase-separated multiblocks composed of polysiloxane blocks and polyimide blocks. Here, using various facets of electron microscopy, we have characterized the domain sizes and elemental composition of these copolymers. *In situ* responses to both thermal annealing and tensile strain have been examined as well. To suggest possible structure–property relationships, differential scanning calorimetry and rheological tests have also been conducted. Measurements are reported for glass-transition and decomposition temperatures, linear viscoelastic properties (storage and loss moduli), and nonlinear stress–strain tensile properties.

## INTRODUCTION

Block copolymers, composed of chemically dissimilar components, are known to undergo microphase separation due to thermodynamic incompatibility between the blocks under certain conditions of temperature, composition, molecular weight, and molecular architecture. The resultant microstructures, or domains, whose sizes are typically on the order of the polymer block end-to-end distances, are responsible for thermomechanical properties that are quite unlike those of either homopolymer or those of a random copolymer with identical composition. Microstructural parameters, such as the domain repeat distance, domain thickness, and the thickness of the interphase existing between the microphases, have been successfully quantified with the use of transmission electron microscopy (TEM),[1-5] small-angle X-ray scattering (SAXS),[6-9] and small-angle neutron scattering (SANS).[10-12] Bulk mechanical and thermal properties, on the other hand, have been well characterized by dynamic mechanical testing (DMT)[13-16] and differential scanning calorimetry (DSC).[17-20] In general, the attempt to discern structure–property relationships in block copolymers has become a major focal point of many research efforts.

*Correspondence should be addressed to: Prof. Michael C. Williams, Dept. of Chemical Engineering, University of California, Berkeley, CA 94720-9989.

Journal of Applied Polymer Science, Vol. 38, 1607–1640 (1989)

CCC 0021-8995/89/091607-34$04.00

Many block copolymers are aimed at providing high-strength materials with bulk properties that allow for facilitated processing. One such copolymer is the poly(siloxane–imide) (SiIm) block copolymer. In this case, the imide polymer offers a wide variety of desirable characteristics. According to King and Lee[21] and Sweeting,[22] polyimides are resistant to irradiation, mechanical deformation, and environmental and solvent attack, while still retaining exceptional thermooxidative and mechanical stability at elevated temperatures. Electrical properties, such as the dielectric constant and volume resistivity, are also insignificantly affected by temperature, thereby making this class of polymer ideally suited for a variety of applications including encapsulant and insulator.[23-26]

As Babu[27] points out, though, polyimides are generally intractable. This problem can be overcome by incorporating a flexible linkage into the polyimide. One successful attempt at doing so is the polyetherimide, which becomes melt processable[28,29] because of the backbone ether link. Another method by which polyimides are made more tractable is the copolymerization with a rubbery polymer such as a polysiloxane. Silicone rubber—polydimethylsiloxane (PDMS)—exhibits temperature stability, oxidative resistance, and physiological inertness, in addition to good electrical properties, but has a tensile strength of only 0.35 MPa. However, a block copolymer composed of both PDMS and imide blocks has been reported to possess a tensile strength of about 50 MPa.[30,31]

In this work, the microstructures of two different SiIm block copolymers are studied by utilizing various techniques of electron microscopy. Thermal and mechanical properties of SiIm cast films are investigated using DSC and DMT.

## EXPERIMENTAL

### Materials

Two SiIm block copolymers are used in this study. The first, produced by M&T Chemicals Inc. (Rahway, NJ 07065) through a polycondensation reaction,[32,33] is the 3510 grade multiblock (designated MT3 for brevity) and is characterized[34-36] in Table I. Described as a polyimide resin,[32-36] this copolymer has the general chemical structure shown in Figure 1. Siloxane blocks, of

TABLE I
Material Properties of the Poly(siloxane–imide) Block Copolymers Used in This Study[a]

| Property | MT3 | GE1 |
|---|---|---|
| Soft-segment content[b] (wt %) | 74 | 40 |
| Molecular weight (g/mol) $\overline{M}_n$ | 50,000–100,000 | 30,000 |
| Glass transition temperature (°C) | 50–58 | — |
| Polydispersity index ($\overline{M}_w/\overline{M}_n$) | 2.0 | 2.0 |

[a] Provided by the manufacturer.
[b] This represents the entire soft segment, including the siloxane and the diamine in the MT3 copolymer and the siloxane block alone in the GE1 copolymer.

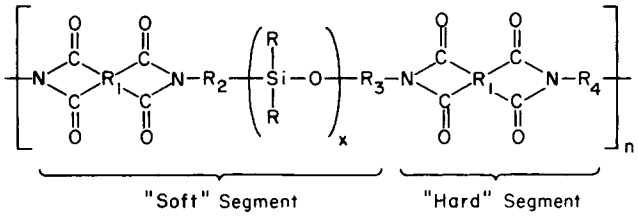


Fig. 1. Chemical structure of an SiIm copolymer, but *not* necessarily the one studied here, produced by M&T Chemicals Inc. The soft segment is comprised of both diamine linkage unit and siloxane block, and the hard segment is a polyimide block. Substituent groups are proprietary and have not been revealed.

the form

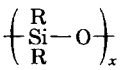

with $x$ essentially constant and of polymeric magnitude (but not divulged), alternate with polyimide blocks. The "soft" segment consists of this siloxane block *plus* a diamine-linkage unit, and the "hard" segment is the imide–anhydride unit $-N(CO)_2R_1(CO)_2NR_4-$. The groups R, $R_1$, $R_2$, $R_3$, and $R_4$ (see Fig. 1) have not been revealed by the manufacturer, though we will offer some speculation below. The sample was received in a 25% solution of *N*-methyl-2-pyrrolidone (NMP); dilute solutions were prepared with dry NMP and were used to cast films (see below) in a dry nitrogen atmosphere. NMP evaporation was conducted according to a cure cycle suggested by the manufacturer (1 h at 100°C, 1 h at 150°C, and 1 h at 200°C), except where noted.

The second copolymer (GE1), a prototype produced by General Electric Co. (Pittsfield, MA 01201), is a multiblock copolymer with varying numbers ($x$ = 10–15) of

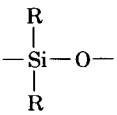

units in the siloxane blocks. Characterization data[37] are presented in Table I. The parent polyimide is the ULTEM-1000 polyetherimide, the structure[29] for which is presented in Figure 2. Chloroform was used to dissolve the copolymer at room temperature.[29,37] Chloroform solutions were prepared to cast thin films, with solvent evaporation performed under the same conditions as above, although no "curing" was specified by the supplier.

## Electron Microscopy

For conventional (low-voltage) transmission electron microscopy and analytical electron microscopy, ultrathin films or sections less than 100 nm thick are required. In this work, ultrathin films approximately 35 nm thick[3] were prepared by using a direct-casting technique (presented elsewhere[38]) from 0.5% solutions of both the MT3 and GE1 copolymers. [For slightly thicker

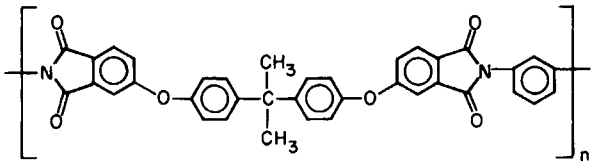

ULTEM-1000

Fig. 2. Chemical structure of the parent polyetherimide, ULTEM-1000, of the GE1 SiIm block copolymer. The ether linkages, in addition to the siloxane, afford this polyimide added flexibility.

GE1 films, 1.0 and 2.0% solutions were needed.] The casting surface was a vapor-deposited carbon layer supported by a Formvar film 10 nm thick which was itself cast upon copper TEM grids of 300 mesh. Since sufficient electron-absorption contrast exists between the imide and siloxane phases, staining was unnecessary. Static and stereo bright-field micrographs were obtained using a JOEL JEM 100CX electron microscope (JOEL Ltd., Peabody, MA 01960) at various magnifications with an accelerating voltage of 80 keV. Micrographs showing the *in situ* curing nature of the MT3 copolymer were also acquired from this microscope with a heating stage attachment.

Direct observation of *in situ* deformation of SiIm microstructures in each copolymer was accomplished by utilizing the capabilities[39] of the KRATOS 1.5 MeV electron microscope at the National Center for Electron Microscopy (Lawrence Berkeley Laboratory). Copolymer films were cast onto the 100-vertical (or horizontal)-mesh copper grid used with a strain stage, depicted in Figure 3. Since Formvar was not used to provide support for the cast film, thicker sample films were required to be self-supportive; such films could still be examined using the greater accelerating voltage of the KRATOS microscope. Once films measuring approximately 200–250 nm thick were cast from 2.0% solutions onto the grid attachment, the stage, which was designed to be completely reusable, was fitted into the straining attachment of the microscope. The sliding tracks and grid attachment were held in place by M-Bond 600 (Measurements Group, Raleigh, NC 27611), a solvent-thinned epoxy-phe-

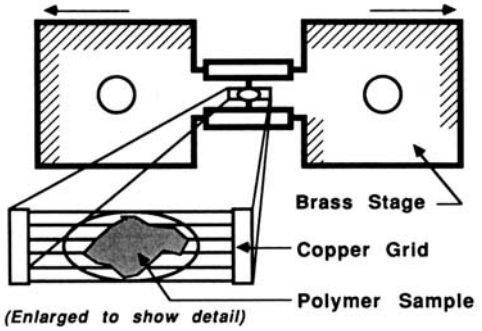


Fig. 3. Schematic diagram of the straining holder used in conjunction with the straining stage on the KRATOS 1.5 MeV electron microscope. The brass plates slide along glide tracks, glued to one plate with an epoxy–phenolic adhesive. Polymer films are cast directly onto trimmed copper grids and are strained as the grids are stretched apart.

nolic adhesive. Tensile deformation at ambient temperature was performed at an elongation rate of 0.11–0.12 μm/s, for periods of time up to 25 min.

Elemental analysis of the GE1 copolymer was accomplished using energy dispersive X-ray microanalysis on a JOEL JEM 200CX analytical electron microscope, operated at an accelerating voltage of 200 keV and equipped to use either a Kevex (Foster City, CA 94404) high-angle detector (HAD) or a Kevex ultrathin-window detector (UTW). The former, having a beryllium window, is able to detect only elements with atomic masses greater than sodium. The latter, with a parylene/aluminum window, is capable of detecting elements as light as carbon. To obtain a representative collection of light-element X-rays (e.g., carbon, oxygen, and nitrogen), samples were cooled in the microscope to −168°C with liquid nitrogen. Due once again to the lower voltage, ultrathin films were required.

### Bulk Analyses

Thick films needed for DSC were prepared in much the same way as the ultrathin films. Here, concentrated solutions (25% for MT3 and 8% for GE1) were repeatedly cast until the desired thickness (≈ 0.5 mm) was attained. A Mettler FP84 differential scanning calorimeter (Mettler Instrument Corp., Hightstown, NJ 08520), set on scan rates of 5°/min and 10°/min, was utilized to discern the thermal behavior of blocks cut from these films.

Both stress–strain and DMT were performed on the MT3 copolymer. An MTS hydraulic testing apparatus (Minneapolis, MN 55424) was used to determine the stress–strain relationships of both the fully cured and partially cured copolymers: the former was cured according to the suggested cure cycle, and the latter was cured for 2 h at 85°C and 2 h at 120°C. [The latter temperature was selected to be below the visibly detected yield temperature[†] of 130°C.] In both cases, the samples were cast from the as-received concentrated 25% solution onto Teflon to avoid adhesion difficulties. The resulting thick films, trimmed to resemble flat, rectangular sheets, measured approximately 0.5 mm in thickness for each sample studied. Sample thicknesses were measured with a micrometer. DMT was conducted with similar samples, using a Rheometrics Mechanical Spectrometer RMS-705 (Piscataway, NJ 08854). Measurements were made at temperatures up to 300°C in a dry nitrogen atmosphere using parallel plates, 25 mm in diameter and separated by 0.8 mm.

## RESULTS AND DISCUSSION

### Microstructural Characterization

Most previous studies of block copolymers have employed diblock and triblock molecules with nominally monodisperse molecular weights. We cannot expect *a priori* the same type of microstructure and properties from polydisperse multiblock copolymers which also are complicated by possessing composition distributions. For instance, Figure 4 shows the fully developed

[†]Weights ranging from 10 to 50 g were suspended from films at ambient temperature. Upon heating, the films began to flow at 130°C, designated as the yield temperature.

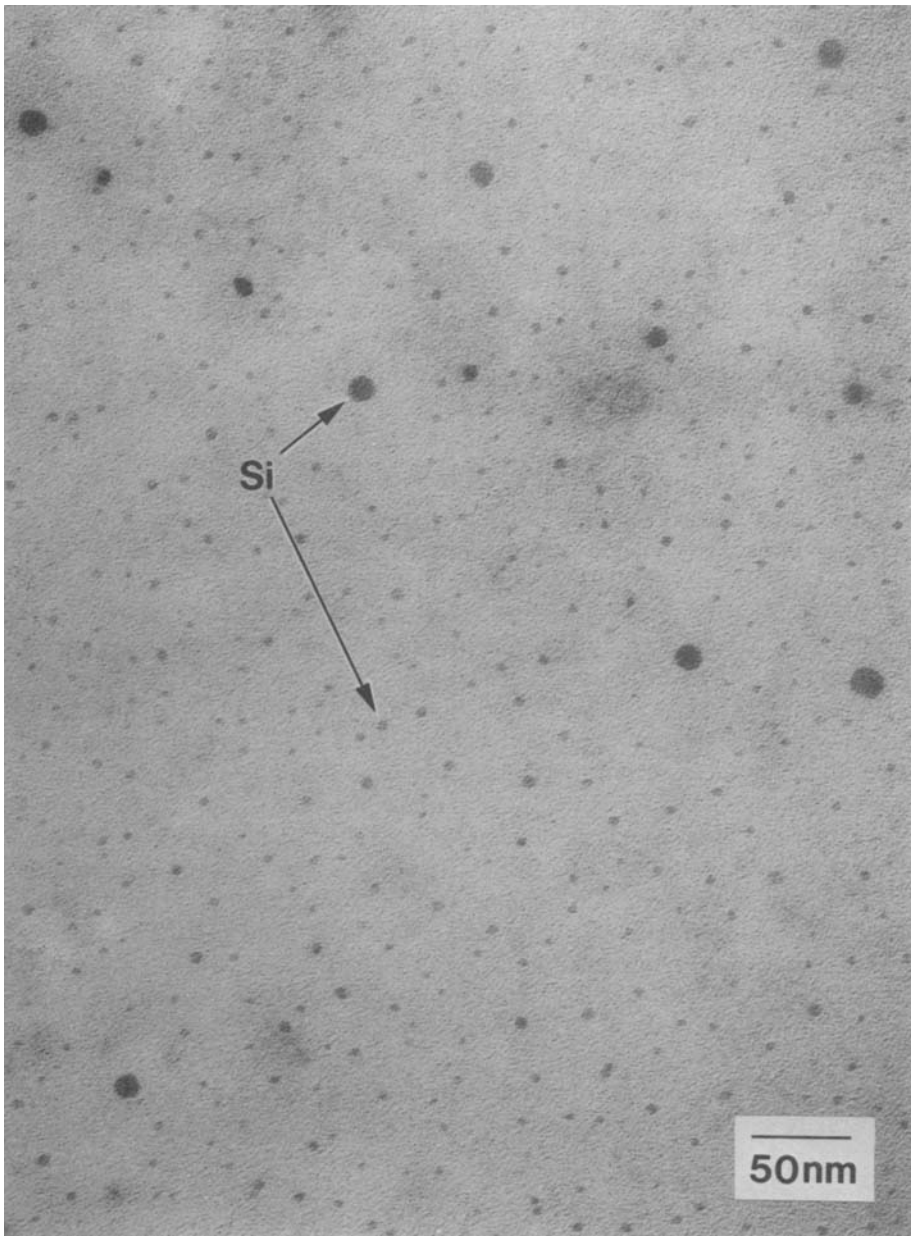


Fig. 4. Electron micrograph of the MT3 copolymer taken with a JEOL JEM 100CX electron microscope. The siloxane microstructures, seen as randomly ordered dark dots, exhibit a somewhat bimodal size distribution, with large domains being approximately 16 nm in diameter and the smaller ones about 5 nm in diameter.

microstructure in the MT3 copolymer after being fully cured. The dispersed domains are identifiable as being Si-rich because of their darkness. This rather small volume fraction of pure siloxane is not inconsistent with the soft segment constituting 74 wt % of the entire copolymer; these two facts together reveal that the siloxane is a minority component within the soft segment but has sufficiently long chains to segregate and form their own

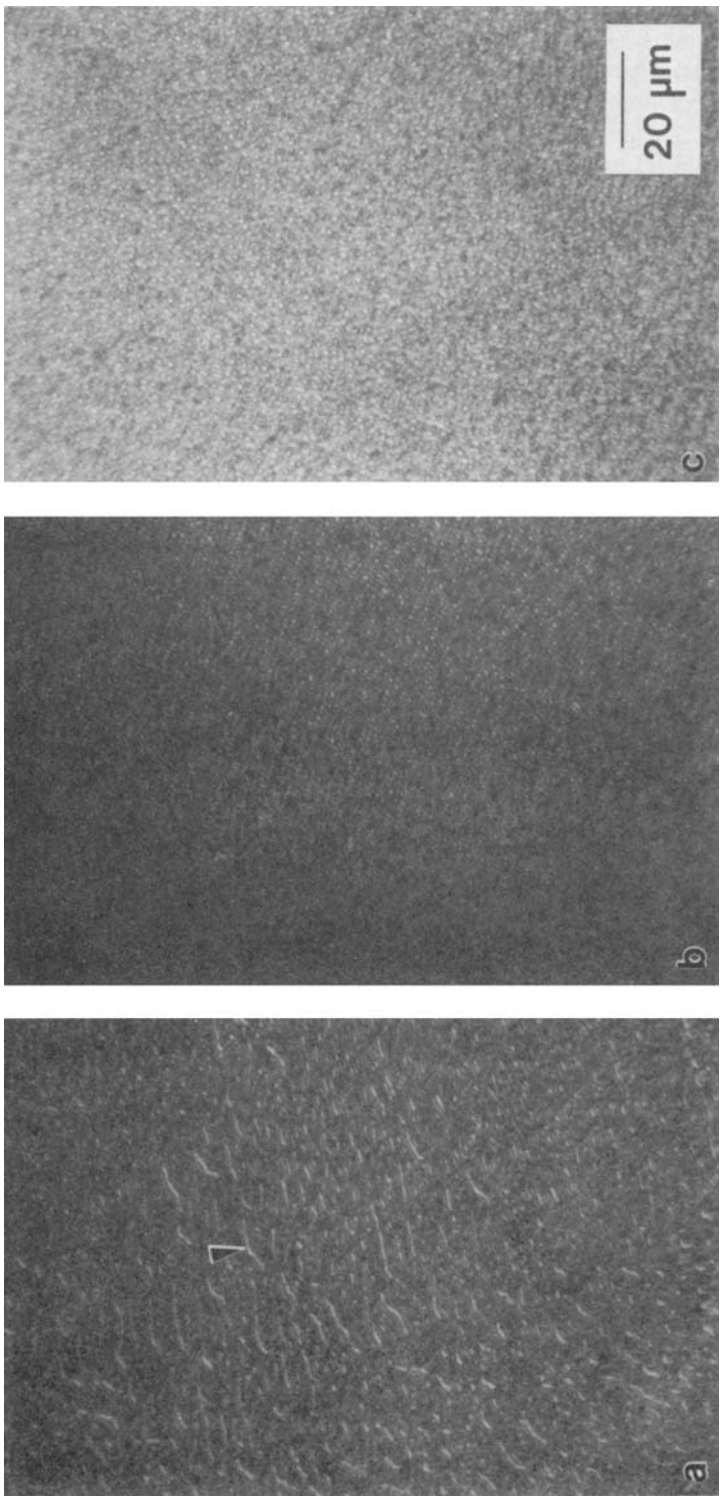


Fig. 5. Optical micrographs, acquired using Nomarski differential contrast spectroscopy, of the GE1 copolymer as a function of casting solution concentration (and, subsequently, film thickness). Globular stretching (see arrow) is observed in (a), which represents a 0.5% solution. These traces are not seen in (b) or (c), which correspond to 1.0 and 2.0% solutions, respectively.

miniphase domains. (Larger domains involving the entire soft segment may exist, but the micrograph cannot reveal it.) A roughly bimodal size distribution of spherical domains is present, with the domain diameters averaging approximately 2–5 and 16 nm in diameter. No hierarchical ordering of the domains is readily noticeable. Collectively, these features of domains are indicative of thermomechanical properties different from those exhibited by monodisperse diblock/triblock copolymers, which possess domain uniformity and well-established ordering.

Unlike the MT3 copolymer, the GE1 copolymer, when cast into ultrathin films, exhibited structure that was visible with an optical microscope and produced haziness in the film. Nomarski differential contrast microscopy,[40] with reflected light at a magnification of 220 $\times$, was used to acquire the micrographs presented in Figure 5. Microstructures appear to vary as the concentrations of solutions used to cast the films in Figure 5 were increased from 0.5% (a) to 1.0% (b) to 2.0% (c). One noticeable difference between Figure 5(a) and Figures 5(b) and 5(c) is that most of the domains in Figure 5(a) seem to have combined or stretched into elongated structures. Additional detail is provided by a series of TEM micrographs (Fig. 6) on similar samples. Again, there is a systematic change of microstructures as the casting-solution concentration increases—i.e., as film thickness increases. The thinnest film [Fig. 6(a)] shows cocontinuous elongated major phases (with an encapsulated miniphase) which gradually changes to large dispersed spherical (or cylindrical) phases [Fig. 6(c)] having thin interconnecting webs or ripples in the film. There is a corresponding change from a lateral orientation to isotropy. Such behavior is highly suggestive of dimensional constraints being imposed on the phase separation process. That is, a microphase whose (bulk) equilibrium configuration contains domains as large as seen in Figure 6(c) will not be able to form such structures in films thinner than they (the structures) are. It is widely recognized, as well, that there are unique surface-energy effects in a film which is thinner than its equilibrium critical thickness,[41] the minimum sample thickness in which equilibrium structures can exist and retain properties of the bulk material.

The sizes of the domains in the GE1 copolymer vary from about tens of nanometers to several microns, which is quite unlike behavior observed in most block copolymers. One plausible explanation for this difference is that the copolymer was designed to have a specified average bulk composition; consequently, the copolymer is composed of polymer molecules having a distribution of compositions (see Table I). Chains with a higher content of the dispersed-phase block would tend to swell the domains much in the same way as a homopolymer would. Another possibility is that simultaneous *macrophase* and *microphase* separation has occurred, in which the former is responsible for large domains and the latter for the small ones. It has been noted for certain polyurethane (segmented, or multiblock, copolymer) systems[42] that heterogeneity in the compositions of molecules was associated with coexisting microphases of greatly differing size scale. This phenomenon has been modeled[43] with the presumption that its origin is a premature phase separation due to reactant incompatibilities during polymerization. Such a model can predict, for example, a bimodal distribution of soft-segment lengths such that these two modes would correspond (if pure) to soft-segment-rich and hard-seg-

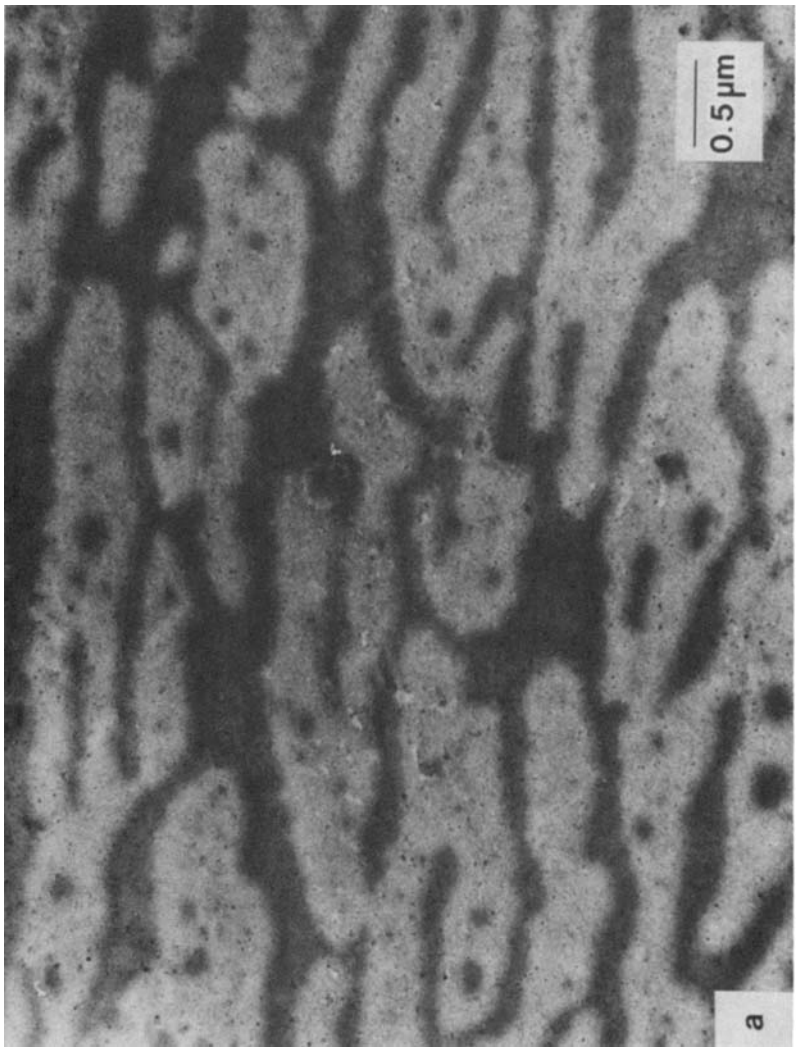


Fig. 6. Electron micrographs of the GE1 copolymer, also as a function of the casting solution concentration: (a) 0.5%; (b) 1.0%; (c) 2.0%. Distinct microstructural deformation, caused by having an ultrathin film that is thinner than the system's critical thickness, is apparent in (a) and becomes less pronounced in (b) and (c).

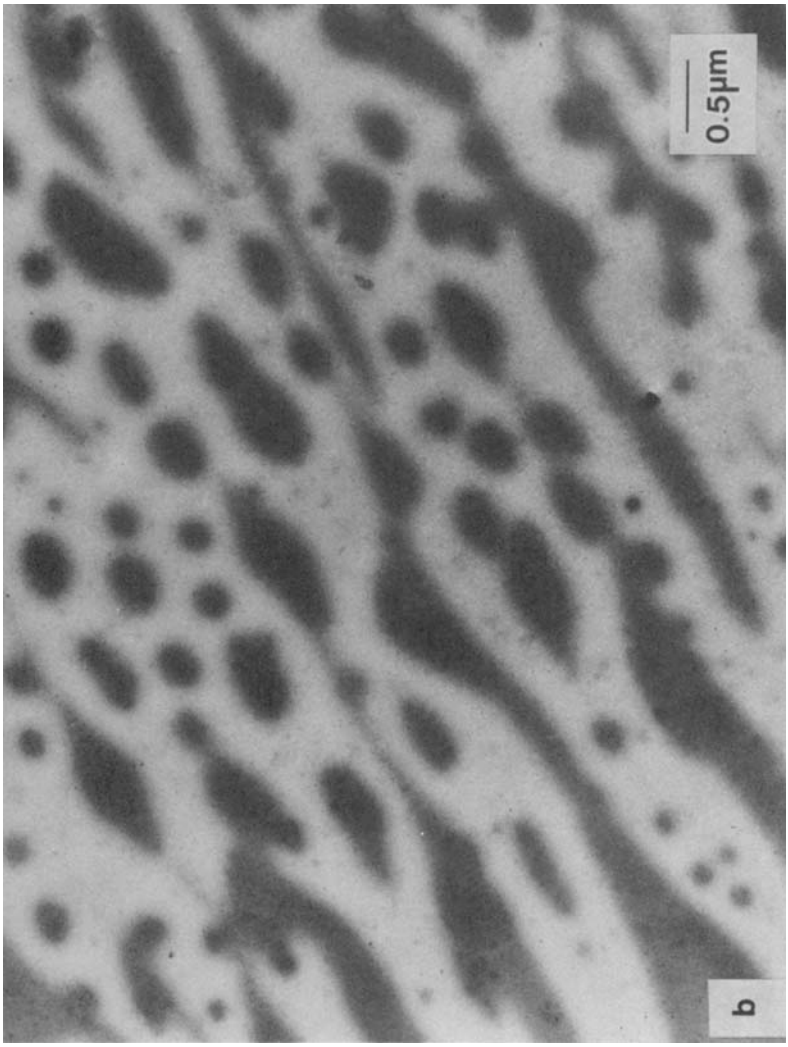


Fig. 6. (*Continued from the previous page.*)

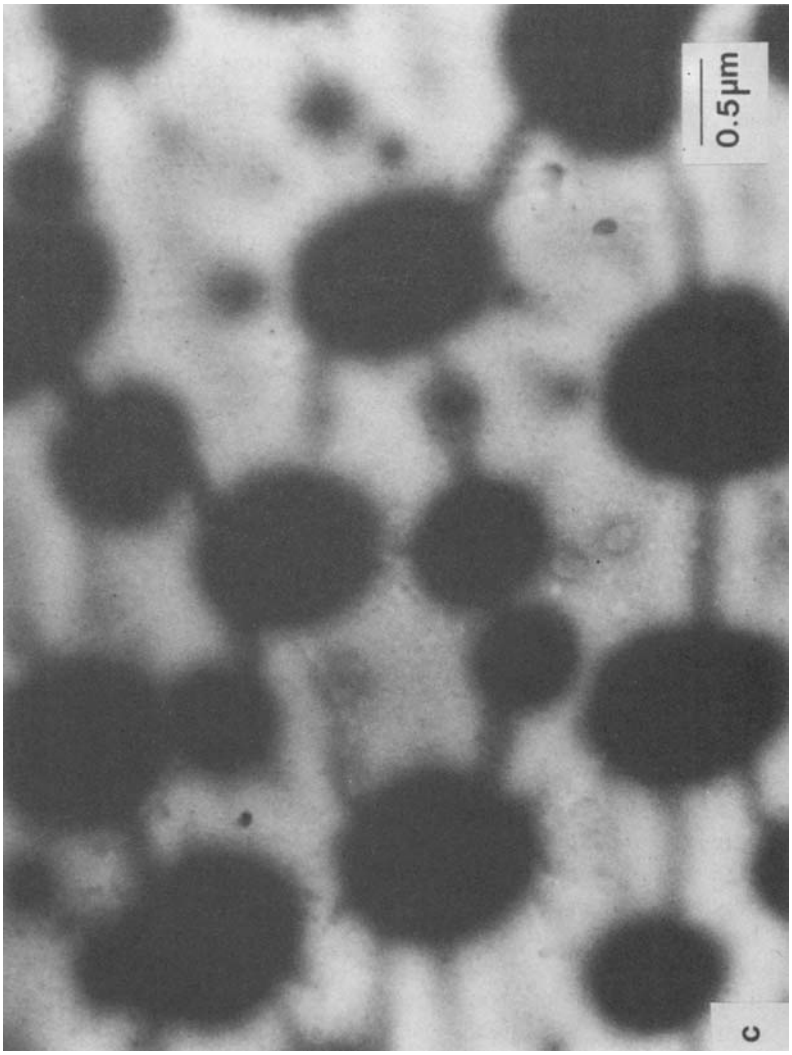


Fig. 6. *(Continued from the previous page.)*

TABLE II
Average Areas and Diameters of the Domains Formed in the GE1 Copolymer as a Function of Casting Solution (Chloroform) Concentration[a]

| Concentration (%) | $\bar{A}_d$ ($\mu m^2$) | $\bar{d}_{eq}$[b] ($\mu m$) | $\bar{d}$[c] ($\mu m$) |
|---|---|---|---|
| 0.5 | 0.070 | 0.299 | 0.225 |
| 1.0 | 0.074 | 0.308 | 0.284 |
| 2.0 | 0.072 | 0.303 | 0.295 |
| Average[d] | 0.072 | 0.303 | 0.260 |

[a] Measurements made with a Numonics Corp. 1224 Electronic Graphics Calculator.
[b] Defined as $(4\bar{A}_d/\pi)^{1/2}$.
[c] Obtained by examining only regular domains appearing two-dimensionally circular.
[d] Found by arithmetically averaging the domain parameters from all the solution concentrations (film thicknesses).

ment-rich materials. The incompatibilities of two such materials in a mixture could give rise to an enormous number of possible microstructural configurations and distributions. It is very likely that the GE1 microstructure is a result of this sort of polymerization chemistry, but such information is proprietary and also beyond the scope of this work.

The size distribution of the resultant domains in the films cast from all three solutions is presented here in several ways. First, the distribution of projected dispersed-phase areas $A_d$ was determined using an electronic graphics calculator manufactured by the Numonics Corp. (Lansdale, PA 19446). This area distribution, which accounts for all discrete albeit irregularly shaped dark domains, is used to determine the domain equivalent diameters from $d_{eq} = (4A_d/\pi)^{1/2}$. Averages of both $A_d$ and $d_{eq}$ are tabulated in Table II. Despite the varying film thickness and obvious morphological differences, the domains have an average $\bar{d}_{eq}$ of approximately 0.30 $\mu m$ in all cases. The median $d_{eq}$ is about 0.18 $\mu m$ in all cases. Upon comparing $\bar{d}_{eq}$ with the average diameter ($\bar{d}$) of domains appearing 2-dimensionally circular, we see that $\bar{d}$ approaches $\bar{d}_{eq}$ at higher solution concentrations and, hence, for thicker films. This indicates that the domains in the thinnest films [Figs. 5(a) and 6(a)] are deformed due to internal stresses arising from the small dimension (thickness) of the film.

In addition to the size distribution of these dispersed domains, a distribution of domain aspect ratios—the ratio of length to width of well-formed domains (i.e., those appearing as 2-dimensional circles and ellipses in micrographs obtained from films varying in thickness)—indicates that more than 70% of these domains have an aspect ratio of between 1.0 and 1.5 upon initial film casting. This information signifies that (a) some internal stresses were produced in the film as the solvent was evaporated but (b) these stresses were not sufficient enough to deform significantly the majority of the domains, especially in the thicker films prepared from the 1.0 and 2.0% solutions (where more "well-formed" domains were present).

Since the siloxane block comprises the minor component of this copolymer ($\approx$ 40 wt %), the domains were initially expected to be silicone-rich. This is what one would also infer from the contrast exhibited between phases; that is,

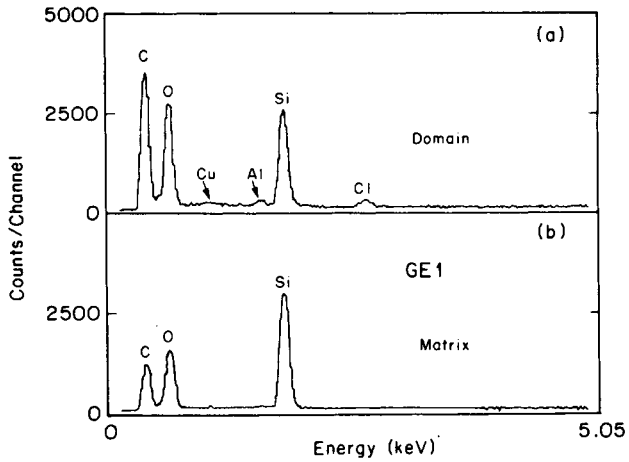


Fig. 7. EDX elemental spectra of the domain (a) and matrix (b) of the GE1 copolymer acquired with an ultrathin window spectrometer operating at −168°C in an analytical electron microscope. The silicon peak is significantly lower in (a) than in (b), whereas the carbon peak is higher in (a) than in (b). This, along with a chlorine peak indicative of residual chloroform solvent which is preferential for the imide block, in (a), suggests that the matrix is siloxane-rich (rubbery) and the domains are imide-rich (glassy). Peaks showing the presence of aluminum and copper are artifacts due to an aluminum holder and the copper support grid.

the siloxane block would normally appear darker due to an increase in the atomic number. However, an elemental analysis of this copolymer using energy-dispersive X-ray microanalysis[44,45] (EDX) on an analytical electron microscope revealed that the matrix, not the dispersed phase, was rich in silicon.

Examples of X-ray spectra for this copolymer are presented in Figure 7. The domain, shown in Figure 7(a), exhibits a higher concentration of carbon than oxygen and silicon, which are about equally present. Chlorine, an artifact from the chloroform solvent, is also present in an appreciable quantity (> 1.0 wt %). In the matrix region [Fig. 7(b)], however, silicon is the most prevalent, followed by oxygen and then by carbon. No chlorine (meaning less than 1.0 wt %) was detected. [Note: Minor, labeled peaks in the spectra of Figure 7 represent copper and aluminum, the former due to the TEM grids and the latter due to the sample holder.] Initial qualitative examination of these spectra indicate that the matrix is siloxane-rich and the domains represent imide-rich regions. An X-ray map of the copolymer is presented in Figure 8 to substantiate this observation. In the lower right corner, a computer-generated image depicts the locations of the domains and matrix. The light areas in the remaining portions of the map illustrate the presence of silicon (upper left), carbon (lower left), and chlorine (upper right). Clearly, silicon is found in greater abundance in the matrix regions, and carbon and chlorine are more prevalent in the domains.

The only way that silicon-lean domains can appear darker than a silicon-rich matrix in transmission (lower right of Fig. 8) is for the domains to be thicker than the surrounding matrix, as shown schematically in Figure 9. Further evidence of this topographical feature is seen upon closer examination of both

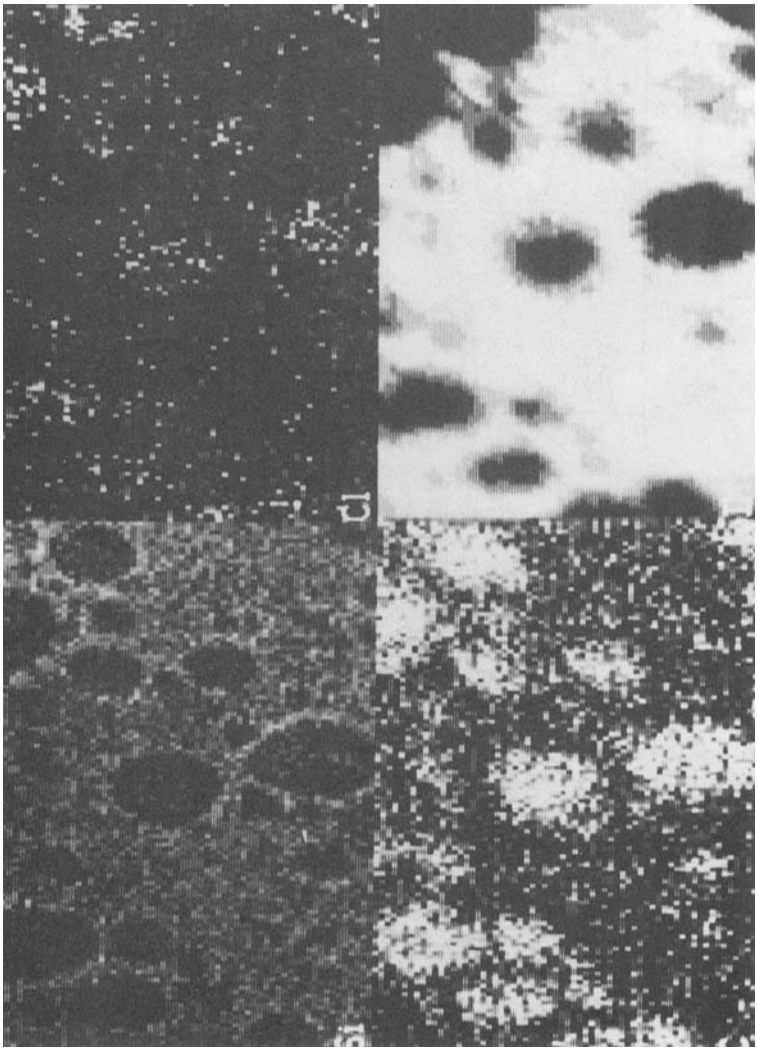


Fig. 8. X-ray map obtained by EDX of the phase-separated GE1 copolymer. The image-enhanced region is seen in the lower right. Comparison of this region with the silicon map (upper left), the carbon map (lower left), and the chlorine map (upper right) verifies the silicon-rich matrix and carbon- and chlorine-rich domains first noticed from the spectra in Figure 7.

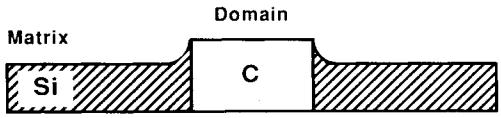


Fig. 9. Domain topography in the GE1 copolymer inferred from a characteristic X-ray map of the domain and matrix regions (Fig. 8). Domains thicker than the matrix appear darker in transmission. Matrix regions adjacent to the domains appear darker in TEM and produce more Si X-rays in EDX than the remaining matrix due to increasing thickness.

the digitized image and silicon map, in which we see a "halo" region surrounding the domains which appears almost as an interphase and which shows a higher silicon content. A stereo view of this copolymer (Fig. 10) reveals definitive features of topography. Domains do, indeed, extend out of the film; and folds, or ripples, are also present. Consequently, we are forced to conclude that (a) the matrix, being siloxane-rich, constitutes the rubbery phase and (b) the domains are imide-rich and provide the stiffness required in this copoly-

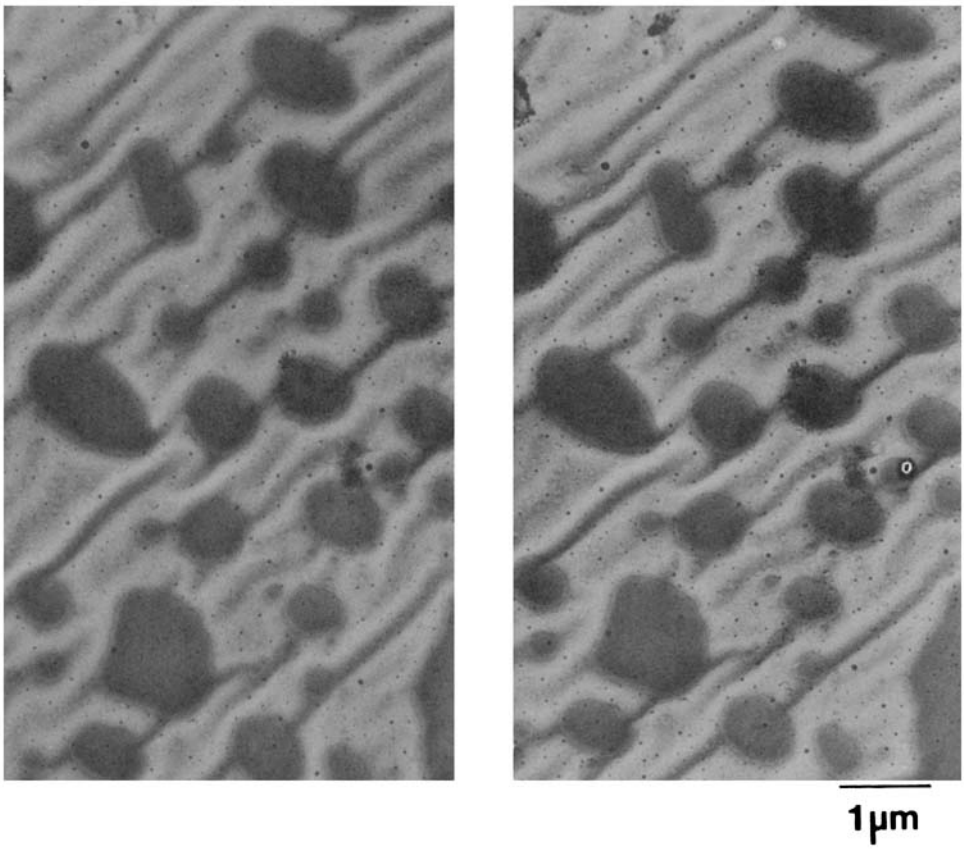


Fig. 10. Stereo pair of electron micrographs of the GE1 copolymer. The micrographs in this pair, obtained by tilting the goniometer stage of the electron micrograph, differ by 10° and, when viewed with a stereo viewer, offer a 3-dimensional representation of the copolymer film. Domains do appear to protrude from the film, and ripples are also present.

TABLE III
$k$ factors Used in the EDX Elemental Analysis[a]

| Element and line | $k$ factor |
|---|---|
| C K$\alpha$ | 4.0000 |
| N K$\alpha$ | 3.5000 |
| O K$\alpha$ | 1.1500 |
| Si K$\alpha$ | 1.0000 |
| Cl K$\alpha$ | 1.0714 |

[a] Experimentally ascertained by Kevex Corp. and the National Center for Electron Microscopy.

mer. The fact that the 40 wt % phase is continuous is explained in part by its larger volume percentage (PDMS is less dense than the imide) and partly by its lesser thickness in the film (Fig. 9). A minority component can, of course, be a continuous phase up to a certain geometrical limit, and this may indeed be thermodynamically favored in some cases. Phase inversion such as this has been reported in ether–amide[46] and styrene–butadiene[47,48] block copolymers.

Quantitative information concerning the composition of the copolymer is acquired from the X-ray intensity counts by relating them to known samples through

$$\frac{C_A}{C_B} = k\frac{I_A}{I_B} \tag{1}$$

where $C$ is the concentration, $I$ is the intensity, A and B represent this sample and a reference sample, and $k$ is the empirical "$k$ factor," values for which, given in Table III, can be obtained by experimental and theoretical means.[45] However, to account for the effects of absorption on the generated characteristic X-rays, $k$ is modified according to

$$k^* = kf(P_z, \rho, t, \alpha_0) \tag{2}$$

where $f$ is a well-characterized function[45] of $P_z$, the absorption coefficient, $\rho$ is the material density, $t$ is the sample thickness, and $\alpha_0$ is the X-ray incident angle. According to the manufacturer,[37] the average density of the siloxane block is estimated to be approximately 1.01–1.05 g/cm$^3$ and that of the imide block to be about 1.15–1.20 g/cm$^3$. (These values are in agreement with the average copolymer density, 1.10 $\pm$ 0.10 g/cm$^3$, of the MT3 sample.[35]) Sample thicknesses are estimated to be about 80 nm.

Compositions, with and without absorption correction, are tabulated in Table IV for both the domain and matrix regions. Absorption corrections are clearly small for this copolymer, and the conclusions reached above concerning phase distribution can now be fully quantified. From the domain to the matrix, the carbon content decreases from about 64 to 46 wt %, whereas the silicon content roughly doubles. Oxygen seems to increase slightly, and the chlorine disappears completely. Further examination of these trends can be accomplished in much the same fashion in an X-ray trace (Fig. 11) across a

TABLE IV
Domain and Matrix Composition Results from the EDX Analysis

| Absorption corrected? | Region | | Composition (%) for elements present[a] | | | |
|---|---|---|---|---|---|---|
| | | | C | O | Si | Cl |
| No | Domain | Weight | 62.02 ± 3.95 | 16.72 ± 0.75 | 19.07 ± 2.71 | 2.18 ± 1.00 |
| | | Atomic | 74.25 ± 2.75 | 15.05 ± 0.93 | 9.80 ± 1.63 | 0.89 ± 0.43 |
| | Matrix | Weight | 42.53 ± 0.64 | 18.82 ± 0.88 | 38.65 ± 1.20 | 0.00 |
| | | Atomic | 58.11 ± 0.57 | 19.30 ± 0.81 | 22.58 ± 0.86 | 0.00 |
| Yes | Domain | Weight | 63.83 ± 3.26 | 16.62 ± 0.76 | 17.51 ± 2.30 | 2.04 ± 0.90 |
| | | Atomic | 75.51 ± 2.20 | 14.77 ± 0.81 | 8.89 ± 1.35 | 0.83 ± 0.38 |
| | Matrix | Weight | 45.60 ± 1.03 | 18.73 ± 0.98 | 35.66 ± 1.68 | 0.00 |
| | | Atomic | 60.87 ± 0.81 | 18.77 ± 0.85 | 20.37 ± 1.17 | 0.00 |

[a] Nitrogen was not detected in appreciable quantities.

domain. The compositions of carbon and chlorine increase from about 45 and 0 wt %, respectively, to about 70 and 1 wt %, respectively, from the matrix to domain and back to the matrix once again. The silicon, however, decreases from about 35 wt % to about 18 wt %. A slight maximum is again observed in the silicon composition between the central portions of the matrix and domain regions.

The fact that silicon is present in both phases presents a curious dilemma, which we now attempt to explain. One possibility for this observed phenomenon is that incomplete phase separation has occurred, as reported for some polyurethane block copolymers.[17,18,49] For instance, by comparing chem-

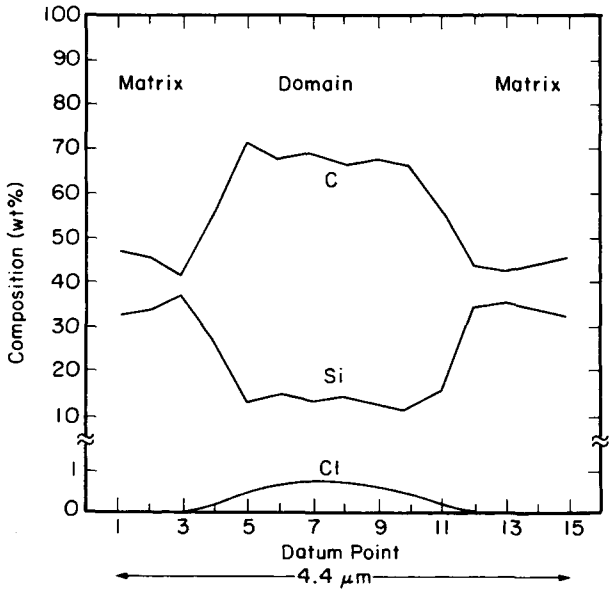


Fig. 11. X-ray trace across a domain measuring approximately 3.2 μm in diameter in the GE1 copolymer. Here, quantification of the silicon, carbon, and chlorine compositions illustrates the degree to which the matrix is silicon-rich and the domains are carbon- and chlorine-rich. Note that the chlorine scale is expanded.

ical nature differences (given as a Flory $\chi$ parameter or a solubility parameter difference) and $\Delta C_p$ measurements, Camberlin and Pascault[17,18] have determined the degree of phase segregation in several polyurethane systems. We can represent the degree of phase separation ($\Delta_S$) in terms of the silicon concentration ($C_{Si}$) in the matrix:

$$\Delta_S \approx \frac{C_{Si}^{mat}}{C_{Si}^{mat} + C_{Si}^{dom}} \tag{3}$$

Here, $C_{Si}$ is expressed in either wt % or atom %, and dom and mat refer to the domain and matrix regions, respectively. Subsequently, eq. (3) yields about $\Delta_S = 0.67$ phase separation using wt % compositions and 0.70 using atom % compositions. This information is useful in predicting macroscopic properties, since such properties are direct functions of phase distribution (which is, in turn, a function of thermodynamics and local-scale kinetics).

The finding that phase separation in GE1 is apparently so far from complete is unexpected. Chemical differences between the blocks are great, leading one to expect a rather complete separation if equilibrium can be achieved. (As a point of reference, we note that segmented polyurethanes incorporating siloxane blocks are reported[18] to have 95% separation of the soft segments.) Two explanations for these results seem viable.

First, it seems reasonable that equilibrium does not prevail. Upon casting from solution, the film establishes a phase-separated microstructure very rapidly because the volatile chloroform solvent vaporizes quickly. This increases the probability that blocks will be kinetically trapped in nonequilibrium configurations. The large size of these phase-separated structures means that the diffusive process toward equilibrium would take a long time. Even annealing to 300°C for short times would have little effect, given the fact that the solvent-free polymer has a $T_g \cong 230$°C (see following section). Thus, either a glassy entrapment mechanism prevails at temperatures of storage and use, or a very high viscosity of imide-rich regions provides diffusive retardance at high temperatures.

Another viable explanation for Si being (apparently) present in both phases is provided by the concept of a thin siloxane-rich layer forming at the copolymer–air interface, which has been reported by others[50] for different SiIm block copolymers. Such a low-energy external layer could form to minimize the free energy of the copolymer system, thus accounting for the silicon being observed by a view from the top of both phases. However, even if this layer was responsible for some of the Si being detected, there is no mistaking the fact that silicon is more highly concentrated in the matrix region.

The most reasonable explanation of the observed silicon distribution is more than likely a combination of these two factors—the formation of a surface siloxane layer *and* incomplete phase separation in the macrophases. Whatever the complete explanation is, the qualitative result remains the same: the matrix is siloxane-rich and is expected to have rubbery characteristics, while the domains are imide-rich and are expected to behave as glassy fillers at room temperature.

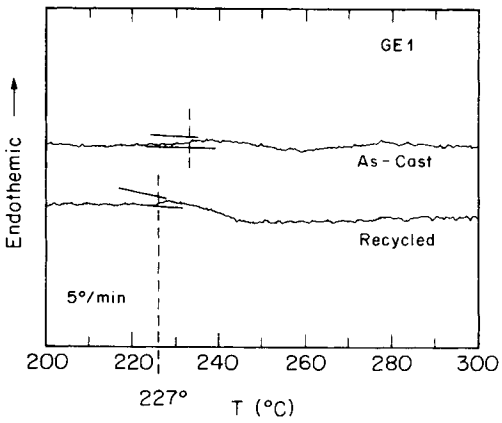


Fig. 12. Differential scanning calorimetry traces of the GE1 copolymer were obtained at a heating rate of 5°C/min on a Mettler FP84 DSC. Here, both the original trace (carried to 300°C) and the trace obtained after recycling the film are presented. The observed $T_g$ in the original sample was at 232°C and that in the recycled sample was 227°C. Upon analyzing several samples, including recycled samples, the average $T_g$ was found to be 227°C. No thermal decomposition was noted.

## Thermal Dynamics

Differential scanning calorimetry traces of the GE1 sample, an example of which is presented in Figure 12, demonstrated a $T_g$ near 227°C. This $T_g$ was completely reproducible upon recycling the sample. In view of the reported[37] $T_g$ for ULTEM-1000 being 215–225°C, we may conclude that the structure in Figure 2 represents the imide block in GE1. The absence of any lower $T_g$ (down to 25°C) suggests that the siloxane block is PDMS. The presence of a pure-imide $T_g$ shows that *microphase* separation occurs very effectively (almost completely), even though it cannot be seen at the size scale of Figures 6 and 8, and supports the concept of a silicon-rich layer existing on the surface of the thin films. In the case of the ultrathin films, a surface layer of Si would certainly explain the apparent detection of Si in both phases; however, the possibility of incomplete phase separation must not be ruled out in light of the earlier discussion on rapid solvent removal.

The recorded $T_g$ for the MT3 copolymer was much lower, approximately 61°C, and was also reproducible upon recycling, as seen in Figure 13. This $T_g$, too, was in agreement with the $T_g$ reported for the copolymer by the manufacturer[35] (50–58°C). Several possible explanations might be devised for this value. One is that $T_g \approx 60$°C represents a blend property, such as an average lying between the high imide value (e.g., 227°C for GE1) and the low siloxane value (e.g., −120°C for PDMS[51] used in GE1). However, this could only be true for a well-mixed blend, and Figure 4 clearly shows phase separation. The second explanation might be that $T_g \approx 60$°C represents the siloxane phase alone, in which case that material might be identified as polydiphenylsiloxane (PDPS), which has $T_g = 62$°C.[51] However, according to the supplier,[36] the siloxane is *not* PDPS. We tentatively conclude that the presence of the diamine, which is invisible in the TEM micrographs, substantially alters the behavior of the siloxane substituents to cause a $T_g$ in the

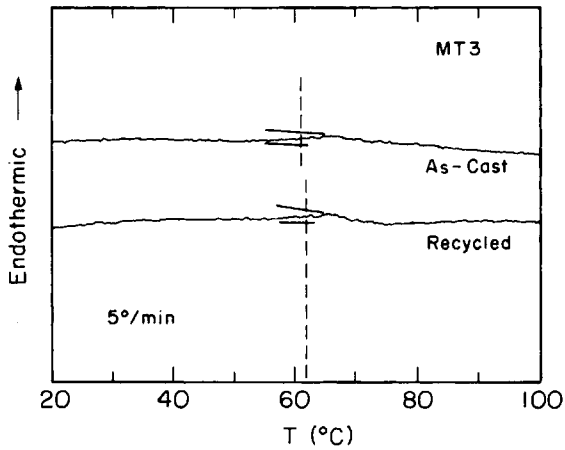


Fig. 13. DSC traces of the MT3 copolymer using the same procedure as described in Figure 12. In both cases, the $T_g$ remains about 60–62°C. Thermal scans were carried to 150°C, and no thermal decomposition was noted.

observed range. The lack of a higher $T_g$ for the imide microphase indicates it is higher than the decomposition temperature, discussed below.

Applications of SiIm copolymers depend on their thermal decomposition temperatures as well as on $T_g$ and curing temperatures. As seen in Figure 14, thermal decomposition of well-cured MT3 is evident beyond 300°C, where the trace indicates the start of an endothermic rise. The reported[35] decomposition temperature is 350°C.

The microstructural response of partially-cured MT3 to temperature, investigated in detail elsewhere,[52] is presented in Figure 15. Unlike the microstructures in the well-cured system, these dispersed microstructures were obtained by heating the MT3 ultrathin film in the electron microscope (with beam turned off) for 15 min at 324.5°C. The fact that film thickness, especially in ultrathin films, has a major impact on thermal processes and stability—e.g.,

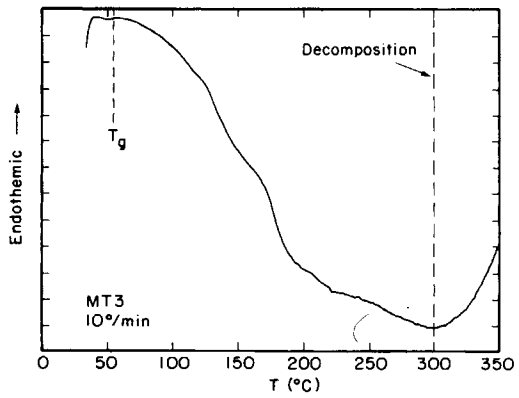


Fig. 14. DSC trace of the MT3 copolymer acquired at a scanning rate of 10°C/min, illustrating both the glass-transition phenomenon and the thermal-decomposition behavior of this copolymer at temperatures above 300°C.

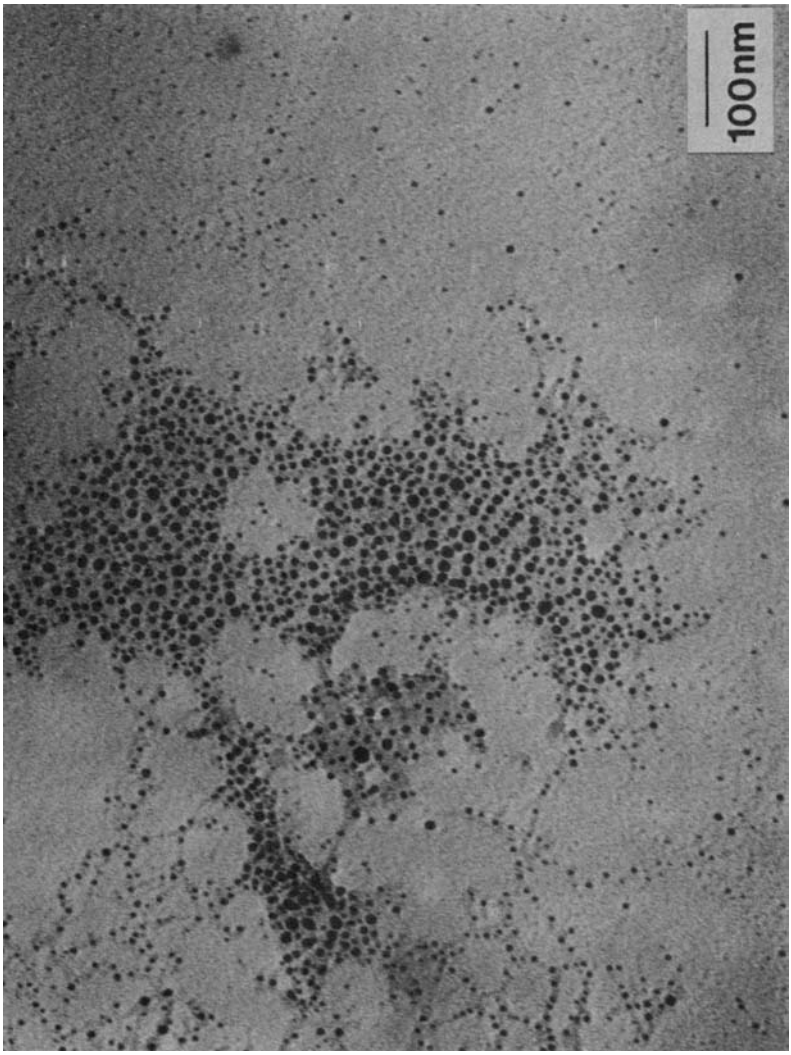


Fig. 15. *In situ* observation of the microstructures in the partially cured MT3 copolymer as the ultrathin film is heated in the electron microscope to 324.5°C for 15 min. The sparse distribution of domains is replaced by heavily populated areas. The size distribution, too, no longer appears to be even approximately bimodal.

spinodal decomposition—is well established; however, the evidence that the siloxane microstructures are responding to an elevated temperature by appearing to coagulate is explicit. The appearance of regions having a significantly higher volume fraction of siloxane domains occurs only above 300°C,[52] suggesting that the relationship between the domains and matrix is being altered at or above this temperature. One reasonable explanation is that either the soft siloxane domains are decomposing (Fig. 14) or the hard imide matrix is becoming soluble in the soft segment. In either case, the biphasic nature of MT3 (characterized by the siloxane–diamine soft segment and the imide hard segment) ceases, except for the siloxane *miniphases* caused by phase incompatibility between the siloxane and diamine blocks within the soft segment. Viscoelastic properties measured at 300°C (see below) seem to substantiate liquidlike behavior in the sense of no interconnected structure. The remaining siloxane domains can then attempt to coalesce (as in Fig. 15), since the matrix is now completely soft.

## Mechanical Dynamics

**I. Microstructural Deformation.** Relating macroscopic mechanical properties to the deformation of microstructures is a desirable goal, but for this purpose the latter should probably not be studied in the context of ultrathin films. Just as with the thermal response of an ultrathin film, the mechanical response of such a film to a strain is also going to contain artifacts related to the film thickness. For example, Boehme and Cargill[53] have shown that anisotropy in a polyimide film, which influences such material properties as the ultimate strength and elongation, increases as the film thickness decreases. Similar findings are evident in the GE1 optical micrographs shown in Figure 5, where anisotropy is clearly evident in the thinnest film (cast from the 0.5% chloroform solution) and also in the TEM micrograph of Figure 6. These problems can be minimized by using high-voltage electron microscopy (HVEM), which permits studying thicker films (e.g., 200 nm), thereby reducing artifacts.

Tensile straining of MT3 thin films (approximately 200 nm thick) at ambient temperature and an elongation rate of 0.11–0.13 $\mu$m/s led to the deformation of microstructures as shown in Figure 16. At time $\tau = 0$, the domains are seen undeformed [Fig. 16(a)]. After 8 min of steadily increasing elongation, the microstructures become distinctly ellipsoidal [Fig. 16(b)]; and after 21 min, the discrete domains have been transformed into continuous striated structures [Fig. 16(c)]. The mechanical response of the polymer chains to the strain is shown schematically in Figure 17, where the imide matrix is shown as the cross-hatched region and the diamine and siloxane portions of the soft segment are presented as the blank (white) and blackened regions, respectively. A multiblock copolymer can interconnect, in principle, the same number of domains as the number of those blocks in the copolymer molecule. However, due to kinetic limitations and looping effects (wherein the molecule retraces itself to place a second block in a domain), the number of interconnected domains is expected to be less than the actual number of these blocks. This latter case is shown in Figure 17(a), where the complexity of interconnected domains under no strain is somewhat simplified to illustrate the

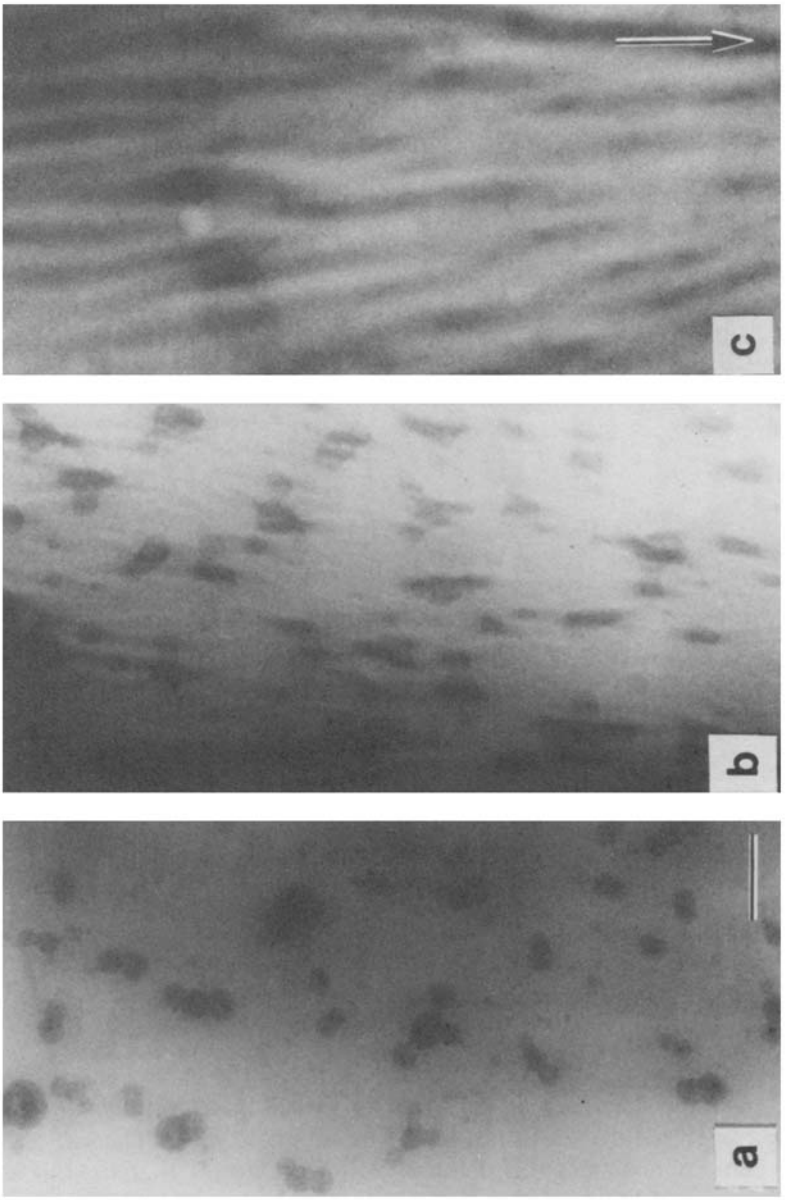


Fig. 16. Real-time sequence of the tensile deformation of siloxane microstructures in the MT3 copolymer. In (a), the domains are under no strain at $\tau = 0$ min. The rubbery domains, normally spherical, become ellipsoidal as strain proceeds for 8 min (b) in the direction of the arrow. Discrete microstructures yield to continuous striations after prolonged strain in (c), where $\tau = 21$ min. Bar in (a) = 20 nm.

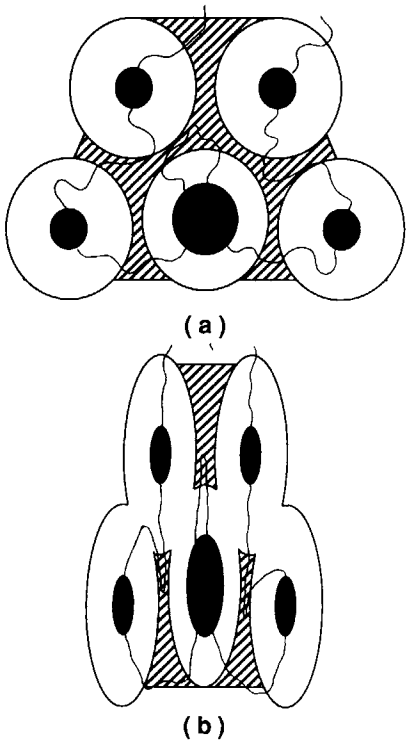


Fig. 17. Schematic representation of the deformation process in the MT3 multiblock copolymer. The complexity of the chain interconnections at rest is illustrated in (a). The polyimide matrix is denoted by the cross-hatching, while the diamine and siloxane portions of the soft block are presented as the blank (white) and blackened regions. Upon initial tensile strain, the rubbery chains within the domains are elongated, thereby distorting the domains. Under continued strain, the rigid imide matrix cracks at points of stress buildup, letting the flexible block endure continued deformation (b). The siloxane domains steadily elongate due to their resiliency and align due to tension in the entire polymer molecule. Fully deformed domains found at varying levels within the film overlap (in transmission) and appear to form striations.

mechanism by which the continuous striations form. As the glassy or possibly crystalline[52] polyimide matrix distorts due to the strain, the rubbery siloxane domains also readily deform, but they do remain interconnected. The soft-segment blocks can accommodate this deformation to the extent that the blocks do not overextend and break. Before this break occurs, the rigid imide matrix will crack, permitting the domains themselves to be pulled into alignment along the axis of strain [Fig. 17(b)]. Continued deformation of the domains occurs with constant straining, and deformed domains from various depths within the copolymer film seem to overlap each other (in projection), thereby appearing to be a continuous, although disordered, lamellar structure. Similar modes of deformation have been reported by Desper et al.[54] who used SAXS to study the response of microstructures of various polyurethanes to tensile strain. They found that the microstructures simultaneously exhibited shear deformation, tensile deformation, and rotation/translation.

When the MT3 film is strained even further than in Figure 16(c), crazes begin to form, an example of which is presented in Figure 18. The crazes,

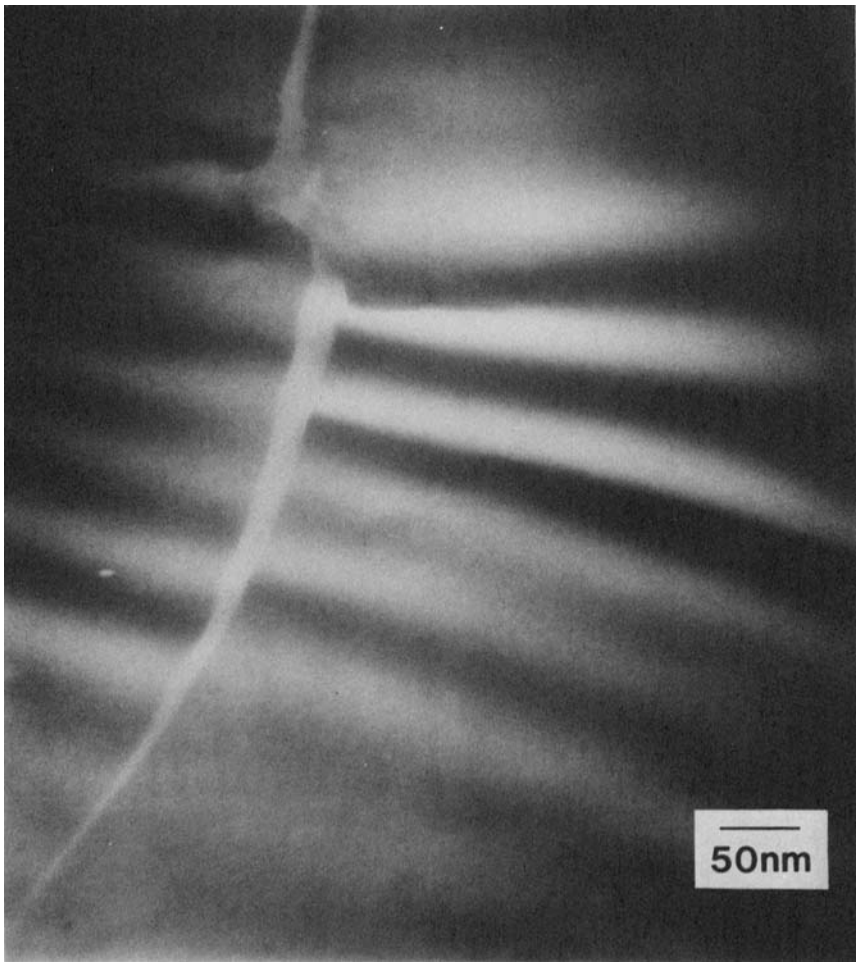


Fig. 18. Electron micrograph of a craze within the MT3 copolymer film. Close examination reveals that the striated structure found in Figure 16(c) appears on both sides of the craze, suggesting that the film reached its maximum stress and then crazed.

cracklike defects which are still load-bearing due to remaining fibrils,[55] are found to be oriented normal to the axis of strain. This is in agreement with the HVEM work of Michler,[56] who studied mechanical microprocesses in several high-impact polymers. In addition, closer examination of Figure 18 reveals that the continuous striations appear on both sides of the craze, indicating that the craze occurred only after the microstructures had adsorbed a sufficient amount of strain energy.

Since the GE1 copolymer has a rubbery matrix and a glassy domain structure (remembering that phase separation is *not* 100% complete), the response of this copolymer is expected to be very different from the MT3 copolymer. Since the GE1 matrix is primarily rubbery, tensile strain will readily deform the matrix; however, despite matrix distortion, the domains will resist deformation. The micrograph in Figure 19, taken at 25°C and under the same strain conditions as the MT3 copolymer in Figure 16(c) (i.e.,

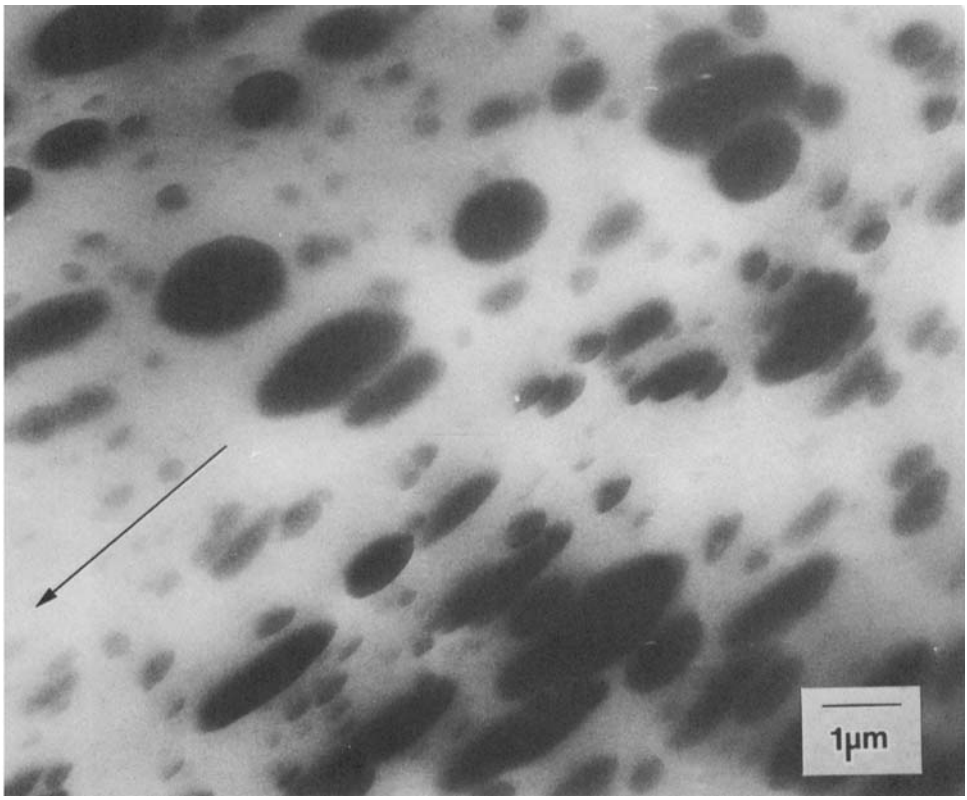


Fig. 19. *In situ* observation of the deformed domains obtained by straining the GE1 copolymer for 20.5 min [as in Fig. 16(c)] in the direction of the arrow. Since these domains, unlike those in the MT3 copolymer, are glassy, tensile deformation is resisted while the rubbery matrix is distorted.

0.11–0.13 $\mu$m/s and $\tau = 21$ min), clearly illustrates this deformation resistance. Even after 21 min of strain, the domains, although deformed, remain discrete. As in Figure 17 for MT3, the microstructures in the GE1 copolymer are expected to deform and then align due to the rubbery matrix. Once again, the chains within the domains are extended due to the imposed strain; however, the extent to which these chains extend is inhibited by the glassy nature of the domains. Before such great extension can occur, the forces on individual glassy-block chains can apparently build up high enough to pull these chains from their domains under continued strain.

**II. Mechanical Properties.** Rheological studies were conducted on the MT3 copolymer only. In the first set of studies, tensile stress–strain relationships of both the fully and partially cured copolymer were investigated under ambient conditions at a constant strain rate of 2.54 mm/s. Sample films, each measuring 0.508 mm in thickness, were obtained by casting the as-received 25% solution onto a Teflon sheet. After being cured in dry nitrogen, films having no visible blemishes were trimmed to form rectangular strips, approximately 2.0 cm long and 0.5–3.0 cm wide, which were used to determine the

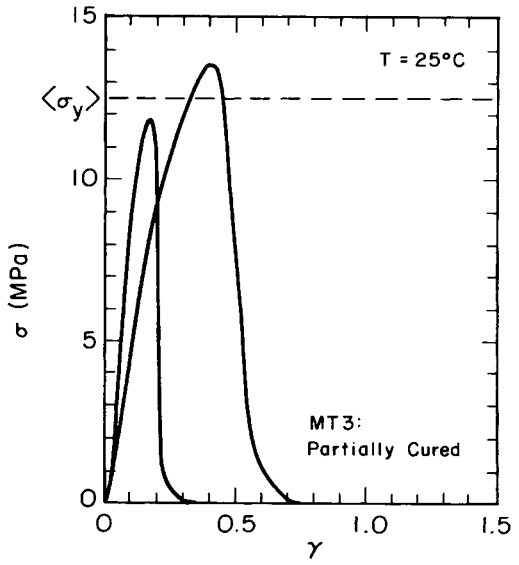


Fig. 20. Bulk stress–strain curves for two partially cured MT3 copolymer samples, acquired at a constant strain rate of 2.54 mm/s on an MTS hydraulic testing apparatus at ambient temperature. After the average yield stress (12.4 MPa) was attained, the sample tore upon further straining. Variations in the curves are due to different sample dimensions.

copolymer's stress–strain properties. For the engineering stress $\sigma$,

$$\sigma(\tau) = F(\tau)/A_0 \tag{4}$$

where $F(\tau)$ is the force imposed as a function of time $\tau$ and $A_0$ is the initial cross-sectional area of the sample. The strain is given by

$$\gamma(\tau) = \delta l(\tau)/l_0 \tag{5}$$

where $l_0$ is the original sample length and $\delta l(\tau)$ is the displacement as a function of time.

The mechanical properties of the partially cured copolymer (cured to 120°C, only) are presented in Figure 20. These two samples reached their maximum stress when $\gamma = 0.15$ and 0.40, and their $\sigma(\gamma)$ curves are not close together. However, they share the feature of failure shortly after the peak stress, and the peak stresses are quite close in magnitude. The average of those peaks is 12.5 MPa, which matches the reported[35] yield stress ($\sigma_y$) for the fully cured copolymer.

In the fully cured sample (cured to 200°C), the copolymer behaved much differently, as seen in Figure 21. The initial segment of the curve represents the actual elastic strain process, identical for the two samples, and ending when yield occurs at $\gamma \approx 0.08$ for one sample and $\approx 0.13$ for another, with an average yield tensile stress of 12.4 MPa. This is followed by an extended draw region (where necking was observed). Each test was terminated when the stress increased again, around $\gamma \cong 0.62$ and 1.04, and the crosshead was

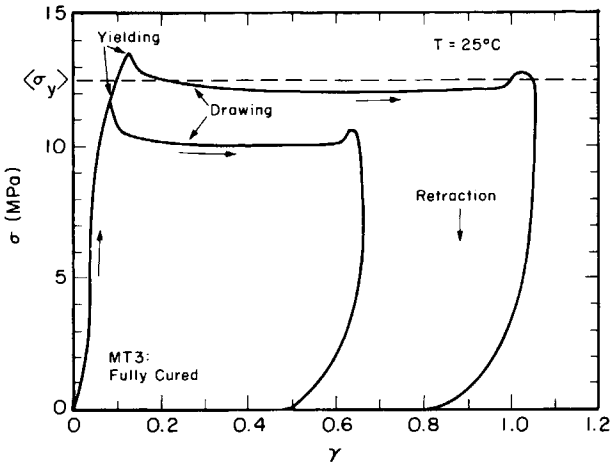


Fig. 21. Stress–strain curves for two samples of the fully cured MT3 copolymer obtained under the same conditions as in Figure 20. The upper portion of each curve indicates the straining process with the first peak, representing the yield stress ($\sigma_y$), occurring at an average of 12.4 MPa. After the yield stress, the samples entered into the plastic region and then exhibited another peak ($\langle\sigma\rangle \approx 11.6$ MPa). Full recovery was observed, as indicated by the lower portion of each curve.

returned to its origin (with the premature zero-load strains indicating the extent of "set"—i.e., plastic flow due to necking). No cracking was observed in these samples. The ultimate tensile stress was also determined for one fully cured sample by straining the sample until it tore apart. We observed this stress to be 14.9 MPa, close to the reported[35] 14.4 MPa.

The major mechanical-property differences between the cured (Fig. 21) and partially cured (Fig. 20) samples are the ductility and toughness—associated with drawability, high stress after yield, and large extensions before failure—conveyed by the curing. Microphase separation has been determined by TEM[52] to occur in both (although less extensively in the partially cured copolymer[52]), as reflected in these data by the equality of low-$\gamma$ peak stresses (12.5 MPa) which presumably signal breakage of the continuous hard phase (rigid polyimide). When such breakage occurs in the uncured samples, structural continuity is entirely lost and macroscopic cracking occurs. However, cured samples apparently have another mechanism to support a load when the imide continuity fails. It may be that curing induces some continuity in the soft (siloxane-rich) phase—which may or may not involve continuity of siloxane chains—or may crosslink it, so that it can better support a load.

DMT studies of the partially cured MT3, conducted at 150°C and above, revealed time-dependent upward drifts in $G'$ and $G''$. This drift, surely caused by continued curing, approached modulus values of the fully cured polymer if allowed to proceed long enough. Behavior of the fully cured sample is given in Figures 22 ($G'$) and 23 ($G''$). These curves were entirely stable with time and also strain-independent up to the highest strain amplitude used (2%).

Interpretation of the rheology at these temperatures is handicapped by not knowing the microstructure, which was determined only near room temperature. However, we know that phase-separated structures persisted to tempera-

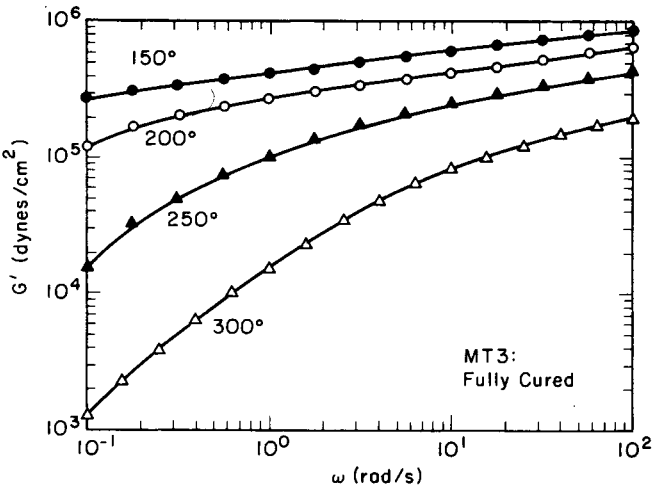


Fig. 22. The dynamic storage modulus ($G'$) of the MT3 copolymer as a function of frequency ($\omega$) at four elevated temperatures (°C): (●) 150; (○) 200; (▲) 250; (△) 300. $G'$ increases with $\omega$ for a given $T$ but decreases with temperature at constant $\omega$, being most sensitive to temperature at the low-$\omega$ threshold.

tures substantially higher than 25°C. The measurement of a $T_g$ at 61°C for the phase-separated system means that the microphase separation temperature $T_s$ must exceed at least 61°C. (Note: 61°C cannot represent the glass transition of a homogeneous non-phase-separated system, or else the microstructure at lower temperature could not form.) Since, according to Leary–Henderson–Williams theory,[47,57] we have $T_s \propto (\delta_{Si} - \delta_{Im})^2$—where the $\delta$'s are pure-block solubility parameters—and $\delta_{Im} \gg \delta_{Si}$, we can expect that two-phase behavior can persist to quite high temperatures. One mitigating

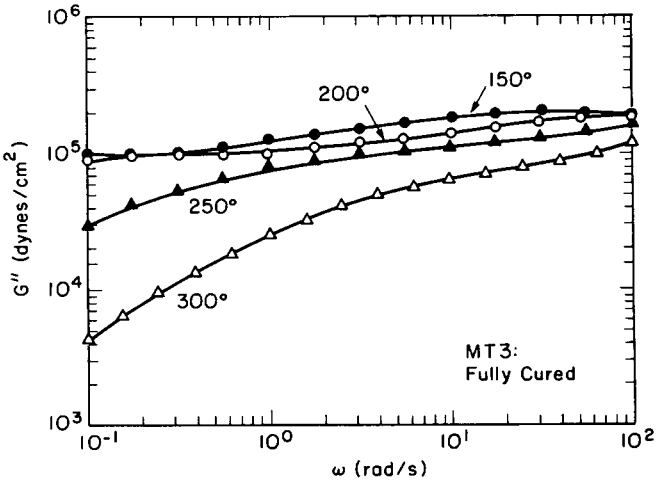


Fig. 23. $G''$ of the MT3 copolymer. $G''$ exhibits the same behavior as $G'$ (Fig. 22), but is almost insensitive to temperature (denoted by the same symbols as in Fig. 22) at the high-$\omega$ spectrum for temperatures up to 250°C.

factor, possibly, is the short length of individual siloxane blocks; for a given chain length, an increase in the number of blocks (i.e., a reduction of block length) seems to reduce $T_s$, if we may extrapolate from tendencies exhibited by diblocks and triblocks.[57] However, the absence of a complete theory for (short) multiblock copolymer microphase separation prevents full evaluation of this factor.

There seems some rheological evidence of the persistence of multiphase behavior to at least 150°C. Figures 22 and 23 show that $G'(\omega)$ and $G''(\omega)$ are almost flat over a wide range of $\omega$—3 orders of magnitude—and have rather high values. The high values could reflect the glassy/crystalline matrix with a dispersed rubbery phase, together with an interconnectedness of domains contributed by participating molecules. The near-independence of $\omega$ is characteristic of entangled systems of very high molecular weight homopolymers and, analogously, interconnected block copolymer domain systems. Furthermore, a limiting value of $G'$ at low $\omega$ is found for all solidlike systems (e.g., crosslinked rubber) and Figure 22 comes close to this at 150°C.

However, such evidence vanishes at higher temperatures, and at 300°C the rheology is comparable to that expected of homogeneous systems. For example, the slope of $G'(\omega)$ at $\omega = 0.1\ s^{-1}$ is about 1.43 and apparently increasing at lower $\omega$. This is very similar to the behavior of homogeneous fluids, all of which must have $G'(\omega)$ approach a low-$\omega$ limiting slope of 2.00 which is rarely reached within experimental conditions (1.5 is very common). Figure 23 gives, at 300°C, a low-$\omega$ $G''(\omega)$ slope of 0.91, close to the theoretical value 1.00 for homogeneous liquids.

Attempts to assemble master curves of $G'(\omega a_T)T_R/T$ and $G''(\omega a_T)T_R/T$ using the time–temperature equivalence principle[58] (TTEP) are shown in Figure 24. Reasonably good superposition is achieved in Figure 24, which uses

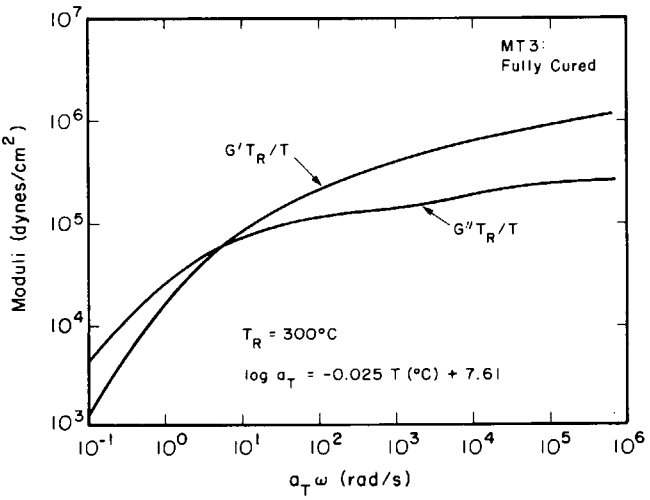


Fig. 24. Master curves of $G'(\omega a_T)T_R/T$ and $G''(\omega a_T)T_R/T$ using the time–temperature equivalence principle[58] (TTEP). Accurate superpositioning was obtained by superpositioning both the $G'T_R/T$ and $G''T_R/T$ data simultaneously. The reference temperature ($T_R$) is 300°C. The logarithm of the shift factor $a_T$ is found to be a linear function of $T$ and is provided in equation form.

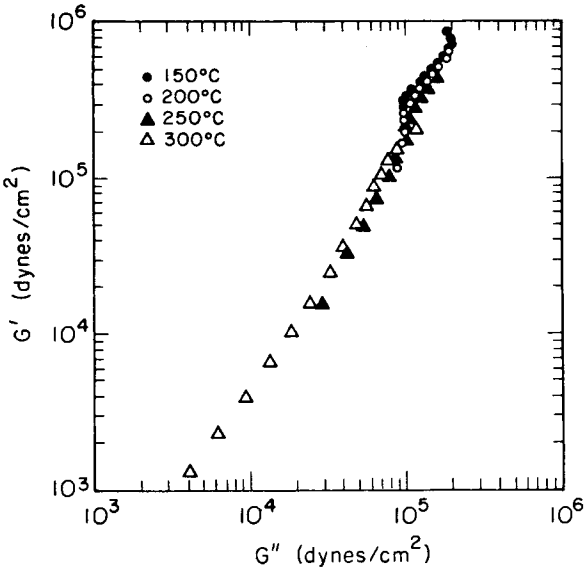


Fig. 25. Plot of log $G'$ vs. log $G''$ to discern a thermally induced phase transition in MT3, according to the method proposed by Han and Kim.[59] (Symbols for data associated with certain temperatures are the same as in Figs. 22 and 23.) Persistence of an inflection in the curve up to 250°C is interpreted as due to heterogeneities associated with microphase separation. The data for 300°C, which just barely extended to the inflection region, seem to show no inflection. Such behavior would suggest that the multiphase microstructure had vanished or greatly weakened at some temperature just below 300°C. This could reflect the onset of decomposition (see Fig. 14), since $T_g$ for the imide microphase is still higher in temperature and $T_s$ could not be seen as long as the glassy imide persisted and prevented diffusion that would lead to homogeneity when $T > T_s$.

300°C as the reference temperature ($T_R$). The linear relationship between log $a_T$ and $T$ (given in equation form in Fig. 24) does not suggest that any transition (e.g., $T_s$) is taking place in this temperature range, but there are not really enough points (temperatures) to be sure. The DSC data in Figure 14 exhibit enough undulation to allow a tentative interpretation that a high-temperature transition—other than decomposition—is taking place. Micrographs[52] such as the one obtained at 324.5°C (Fig. 15) provide evidence that microstructures are markedly different from those seen at lower temperatures (Fig. 4), and, even though they persist (at least for several minutes) to the decomposition temperature in the MT3 copolymer, they may not be thermodynamically stable.

In addition, using the rheological criterion proposed by Han and Kim[59] to determine the microphase-separation temperature in diblock and triblock copolymers, we have constructed a log $G'$ vs. log $G''$ plot (Fig. 25) to ascertain the presence of a thermally induced phase transition. The curves corresponding to temperatures between 150 and 250°C exhibit an inflection, which is not characteristic of a homogeneous polymer. The higher-temperature curve (300°C) does not possess this characteristic, suggesting that the solidlike microstructural features of MT3 at lower temperatures are no longer present. If this inflection represents some microstructural effect due to phase separation between the diamine-siloxane soft segment and the imide hard segment,

then the absence of the inflection reflects the end of stable phase separation (due, for example, to decomposition or increased diamine–imide solubility).

## CONCLUSIONS

Characterization of the microstructures existing in two phase-separated poly(siloxane–imide) multiblock copolymers, in addition to bulk thermal and mechanical properties, has been established. Because the development of incorporating silicone blocks in polyimides is still so recent, little work has focused on the structure–property relationships in these new multiblock, or segmented, copolymers. Using conventional (low-voltage) transmission electron microscopy, we characterized the size of these microstructures in both the MT3 and GE1 copolymers, the former having siloxane domains on the order of 5 and 16 nm in diameter and the latter having a distribution of domain sizes including some very large (order of micrometers). Energy-dispersive X-ray microanalysis (EDX) was utilized in discerning the compositions of the phases in the GE1 sample; subsequently, we found that the matrix appeared to be rich in silicon, even though the sample is only 40% siloxane by weight. Interpretation of the observed phase separation led to three possible explanations: (1) the EDX results accurately represented the copolymer, thereby indicating incomplete phase separation with $\Delta_S \approx 0.67$–$0.70$, (2) a silicon-rich layer existed on the surface of the film, providing evidence for silicon to be present in both phases, or (3) a reasonable combination of (1) and (2). In either of these cases, the matrix was still rich in silicon, and the dispersed domains remained imide rich.

Dynamic TEM was successfully utilized in studying both the thermal and mechanical responses of the microstructures present in the copolymers. The domains in the MT3 sample, when heated near the thermal decomposition temperature ($\approx$ 300–350°C), changed dramatically in appearance and resembled liquidlike droplets. Responding to tensile strain in the KRATOS high-voltage electron microscope, the microstructures of both copolymers exhibited deformation: the MT3 domains elongated to form continuous striations after about 21 min of strain, and the GE1 domains distorted far less after the same degree of strain due to their glassy nature.

Bulk material properties were analyzed using DSC and DMT methods. Glass-transition temperatures were found for both copolymers. The $T_g$ of the MT3 sample was about 61°C and that of the GE1 sample about 227°C (which is comparable to that of the parent polyetherimide, ULTEM-1000). Bulk mechanical properties of the MT3 copolymer at room temperature demonstrated variations with respect to the cure cycle of the sample. For samples only partially cured, the yield stress ($\approx$ 12.4 MPa) was attained at strains under about 0.4, but the sample tore beyond this. In the fully cured samples, this stress was achieved and followed by a plastic-flow regime to strains as large as 1.0 without breaking. The ultimate stress, reported[35] as 14.4 MPa, was measured here at about 14.9 MPa.

Dynamic mechanical tests at elevated temperatures also showed differences between partially and fully cured MT3 samples. In the former, storage and loss moduli were unstable and increased with time, as curing proceeded during the test. In the latter, both moduli were completely reproducible at any

measured temperature and were insensitive to the strain amplitude (between 1.0% and 2.0%). Application of the TTEP[58] to create master curves of $G'(\omega a_T)T_R/T$ and $G''(\omega a_T)T_R/T$ yielded good superpositioning, with $\log(a_T)$ decreasing linearly with temperature. Such superpositioning did not suggest a phase transition (e.g., $T_s$) between 150 and 300°C. However, an inflection in a plot of log $G'$ vs. log $G''$ for all temperatures as high as 250°C may reflect the existence of microphase separation. This inflection seemed to be absent at 300°C, suggesting that a transition (perhaps decomposition) was occurring near this temperature.

The authors would like to thank L. J. Male of General Electric Co. and R. Eddelman of M&T Chemicals Inc. for the block copolymer samples, C. Schooley and D. Davis of the Electron Microscope Laboratory (University of California, Berkeley) for guidance in TEM operations, D. Ackland and C. Echer of the National Center for Electron Microscopy (Lawrence Berkeley Laboratory) for assistance in the HVEM and EDX analyses, and D. Boyington and D. Kalika for help in performing the mechanical property tests. This work was supported by the Director, Office of Energy Research, Office of Basic Energy Sciences, Materials Science Division of the U.S. Department of Energy under Contract No. DE-AC03-76SF00098.

## References

1. F. Annighofer and W. Gronski, *Makromol. Chem.*, **185**, 2213 (1984).
2. R. J. Spontak, M. C. Williams, and C. N. Schooley, *J. Mater. Sci.*, **21**, 3173 (1986).
3. R. J. Spontak, M. C. Williams, and D. A. Agard, *Polymer*, **29**, 387 (1988).
4. R. J. Spontak, M. C. Williams, and D. A. Agard, *Macromolecules*, **21**, 1377 (1988).
5. K. Ishizu, T. Hayashi, and T. Fukutomi, *Makromol. Chem.*, **187**, 689 (1986).
6. R. Mayer, *Polymer*, **15**, 137 (1974).
7. G. Hadziioannou and A. Skoulios, *Macromolecules*, **15**, 267 (1982).
8. T. Hashimoto, M. Shibayama, and H. Kawai, *Macromolecules*, **13**, 1237 (1980).
9. T. Hashimoto, M. Fujimura, and H. Kawai, *Macromolecules*, **13**, 1660 (1980).
10. R. W. Richards and J. L. Thomason, *Polymer*, **24**, 1089 (1983).
11. R. W. Richards and J. L. Thomason, *Macromolecules*, **16**, 982 (1983).
12. F. S. Bates, S. B. Dierker, and G. D. Wignall, *Macromolecules*, **19**, 1938 (1986).
13. T. Hashimoto, Y. Tsukahara, K. Tachi, and H. Kawai, *Macromolecules*, **16**, 648 (1983).
14. J. Diamant, D. S. Soong, and M. C. Williams, in *Contemporary Topics in Polymer Science*, W. J. Bailey and T. Tsurata, Eds., Plenum, New York, 1984, Vol. 4.
15. F. Annighofer and W. Gronski, *Colloid Polym. Sci.*, **261**, 15 (1983).
16. J. Diamant, Ph.D. thesis, University of California, Berkeley, 1982.
17. Y. Camberlin and J. P. Pascault, *J. Polym. Sci., Polym. Phys. Ed.*, **22**, 1835 (1984).
18. J. P. Pascault and Y. Camberlin, *Polymer Commun.*, **27**, 230 (1986).
19. L. M. Leung and J. T. Koberstein, *Macromolecules*, **19**, 706 (1986).
20. K. K. Chee and R. J. Farris, *J. Appl. Polym. Sci.*, **29**, 2529 (1984).
21. J. J. King and B. H. Lee, in *High Performance Polymers: Their Origin and Development*, R. B. Seymour and G. S. Kirshenbaum, Eds., Elsevier, New York, 1986, pp. 317–330.
22. O. J. Sweeting, in *The Science and Technology of Polymer Films*, O. J. Sweeting, Ed., Wiley, New York, 1971, pp. 658–667.
23. A. M. Wilson, in *Polyimides: Synthesis, Characterization, and Applications*, K. L. Mittal, Ed., Plenum, New York, 1984, Vol. II, pp. 715–733.
24. H. J. Merrem, R. Klug, and H. Hartner, in *Polyimides: Synthesis, Characterization, and Applications*, K. L. Mittal, Ed., Plenum, New York, 1984, Vol. II, pp. 919–931.
25. R. Pariser, *Polym. J.*, **19**, 127 (1987).
26. S. T. Kowell, R. Selfridge, C. Eldering, N. Matloff, P. Stroeve, B. Higgins, M. P. Srinivasan, and L. B. Coleman, *Thin Solid Films*, **152**, 377 (1987).
27. G. N. Babu, in *Polyimides: Synthesis, Characterization, and Applications*, K. L. Mittal, Ed., Plenum, New York, 1984, Vol. I, pp. 51–65.

28. J. G. Wirth, in *High Performance Polymers: Their Origin and Development*, R. B. Seymour and G. S. Kirshenbaum, Eds., Elsevier, New York, 1986, pp. 195–205.

29. I. W. Serfaty, in *Polyimides: Synthesis, Characterization, and Applications*, K. L. Mittal, Ed., Plenum, New York, 1984, Vol. I, pp. 149–161.

30. F. W. G. Fearon, in *High Performance Polymers: Their Origin and Development*, R. B. Seymour and G. S. Kirshenbaum, Eds., Elsevier, New York, 1986, pp. 381–388.

31. C. M. Melliar-Smith, S. Matsuoka, and P. Hubbauer, *Plast. Rubber Mat. Appl.*, **5**, 49 (1980).

32. A. Berger, U.S. Pat. 4,139,547 (1979).

33. A. Berger, U.S. Pat. 4,395,527 (1983).

34. A. Berger, in *Polyimides: Synthesis, Characterization, and Applications*, K. L. Mittal, Ed., Plenum, New York, 1984, Vol. I, pp. 67–75.

35. M & T 3500 Siloxane Polyimide Data Sheet, M & T Chemicals, Rahway, NJ, 1983.

36. R. Eddelman, M & T Chemicals, Inc., personal communications, 1987.

37. J. Male and D. Floryan, General Electric Co., personal communications, 1987.

38. R. J. Spontak, in *Proceedings of the 44th Annual Meeting of the Electron Microscopy Society of America*, G. W. Bailey, Ed., San Francisco Press, San Francisco, 1986, pp. 788–789.

39. *User's Guide*, National Center for Electron Microscopy, Lawrence Berkeley Laboratory, Publication 475, 1987.

40. J. G. Delly, *Photography through the Microscope*, Eastman Kodak, Rochester, NY, 1980, pp. 66–67.

41. E. P. Butler and K. F. Hale, in *Practical Methods in Electron Microscopy*, A. M. Glauert, Ed., North-Holland, Amsterdam, 1981, Vol. 9.

42. M. Xu, W. J. McKnight, C. H. Y. Chen-Tsai, and E. L. Thomas, *Polymer*, **20**, 2183 (1987).

43. J. A. Miller, T. A. Speckhard, and S. L. Cooper, *Macromolecules*, **19**, 1568 (1986).

44. D. Vaughan, *Energy-Dispersive X-Ray Microanalysis: An Introduction*, Kevex Corp., Foster City, CA, 1983.

45. D. B. Williams, *Practical Analytical Electron Microscopy in Materials Science*, Philips Electronic Instruments, Mahwah, NJ, 1984, Chap. 4.

46. M. Xie and Y. Camberlin, *Makromol. Chem.*, **187**, 383 (1986).

47. D. F. Leary and M. C. Williams, *J. Polym. Sci., Polym. Phys. Ed.*, **11**, 45 (1973).

48. R. J. Spontak and M. C. Williams, in *Proceedings, Analytical Electron Microscopy—1987*, D. Joy, Ed., San Francisco Press, San Francisco, 1988, pp. 159–160.

49. J. A. Miller, G. Pruckmayr, E. Epperson, and S. L. Cooper, *Polymer*, **26**, 1915 (1985).

50. C. A. Arnold, J. D. Summers, R. H. Bott, L. T. Taylor, T. C. Ward, and J. E. McGrath, in *Proceedings of the Society for Advancement of Materials and Process Engineering*, April 1987.

51. J. Brandrup and E. H. Immergut, Eds., *Polymer Handbook*, Wiley-Interscience, New York, 1966.

52. R. J. Spontak and M. C. Williams, *Polym. J.*, **20**, 649 (1988).

53. R. F. Boehme and G. S. Cargill, in *Polyimides: Synthesis, Characterization, and Applications*, K. L. Mittal, Ed., Plenum, New York, 1984, Vol. I, pp. 461–476.

54. C. R. Desper, N. S. Schneider, J. P. Jasinski, and J. S. Lin, *Macromolecules*, **18**, 2755 (1985).

55. H. R. Brown, *Polymer*, **26**, 483 (1985).

56. G. H. Michler, *Polymer*, **27**, 323 (1986).

57. C. P. Henderson and M. C. Williams, *J. Polym. Sci., Polym. Phys. Ed.*, **23**, 1001 (1985).

58. D. W. van Krevelen, *Properties of Polymers: Their Estimation and Correlation with Chemical Structure*, Elsevier, Amsterdam, 1976, pp. 289–294.

59. C. D. Han and J. Kim, *J. Polym. Sci., Polym. Phys. Ed.*, **25**, 1741 (1987).

Received August 8, 1988
Accepted August 18, 1988